

Journal of Materials Chemistry A

Accepted Manuscript



This is an *Accepted Manuscript*, which has been through the Royal Society of Chemistry peer review process and has been accepted for publication.

Accepted Manuscripts are published online shortly after acceptance, before technical editing, formatting and proof reading. Using this free service, authors can make their results available to the community, in citable form, before we publish the edited article. We will replace this *Accepted Manuscript* with the edited and formatted *Advance Article* as soon as it is available.

You can find more information about *Accepted Manuscripts* in the [Information for Authors](#).

Please note that technical editing may introduce minor changes to the text and/or graphics, which may alter content. The journal's standard [Terms & Conditions](#) and the [Ethical guidelines](#) still apply. In no event shall the Royal Society of Chemistry be held responsible for any errors or omissions in this *Accepted Manuscript* or any consequences arising from the use of any information it contains.

Ethanol-Directed Morphological Evolution of Hierarchical CeO_x Architectures as Advanced Electrochemical Capacitors

Adnan Younis*, Dewei Chu* and Sean Li

*School of Materials Science and Engineering, University of New South Wales, Sydney, 2052,
NSW, Australia*

*Corresponding Author: Tel.: +61 (0)2 9385 5386; Fax: +61 (0)2 9385 6565

E-mail address: a.younis@unsw.edu.au, d.chu@unsw.edu.au

Abstract

To surmount the fundamental limits of energy density in the current supercapacitor devices, the electrode materials should be capable to store localized charge while having high degree of freedom to provide ease in electrons/ions flow in/out of the electrodes. Herein, we demonstrated a facile approach to design CeO_x based hierarchical architectures for high performance energy storage electrodes. The unique CeO_x based hierarchical architectures, including nanowires, nanocables, nano-micro biscuits and micro walls were fabricated by simply manipulating the nitrate ions oxidation rate during electrochemical synthesis. Among all electrodes, the CeO_x nano-micro biscuits demonstrated excellent electrochemical performance that undergo fast faradaic reactions leading to high specific capacitance within short charging time. Furthermore, voltametric sweep mediated analysis was utilized to quantify the capacitive and intercalation effects in the total stored charge capacity of CeO_x nano-micro biscuits. The presence of higher Ce³⁺ content (as confirmed by XPS studies) in CeO_x nano-micro biscuits could be responsible to accelerate Faradaic redox reactions (conversion of Ce³⁺ to Ce⁴⁺) in electrolyte solution, which is sufficient to realize its superior

performance over other nano-microstructures. The present study demonstrates the effectiveness of CeO_x as a low cost and potentially promising candidate for future energy storage/harvesting and integrated nanoelectronic devices.

Keywords

Ceria, energy storage, oxygen vacancies, supercapacitors

Introduction

With the advancing curiosity in portable energy devices, energy storage is becoming more important than at any instance in the past. Owing to the high power density and excellent cycling capabilities than conventional rechargeable batteries, supercapacitors have gained considerable attention as a fast-rising class of energy-capture and storage devices with safe operation and fast charging/discharging rates¹⁻³. Today, improving energy density without sacrificing the power density and cyclic lifetime has become a greater challenge for the supercapacitor industry.

Supercapacitors are generally classified into electric double-layer capacitors (EDLC)^{1, 4} and pseudocapacitors⁵ depending on their charge storage mechanisms. Contrary to non-Faradic EDLC, the pseudocapacitors store charges by a Faradic process through redox reactions at the interface between the electrolyte and electrode, therefore possess larger capacitance and higher energy density than EDLC. The capacitance performance of pseudocapacitors mainly depends on the availability of active electrode materials that should possess characteristics such as high surface area, porous network, long-term stability, cyclability and high rate of electrochemical oxidation/reduction⁶. In past, owing to high pseudocapacitance performance, the transition metal oxides/hydroxides being redox-active materials are widely chosen as electrode materials⁷. In general, the surface area and

morphology are the two most influential parameters for determining pseudocapacitive performance of metal oxides. For approaching high capacitance values, high surface area has always been an important consideration because high surface area can provide more active sites to facilitate the charge/discharge processes. However, the role of surface area is crucial to a certain extent, beyond its limits some other factors (particularly; pore size/volume) may also contribute significantly in ions transportation for charge storage capabilities of an electrode. Therefore, to achieve a superior performance, it is essential to structurally control the design of electrode materials with optimized pore volume as well as surface area.

In the present study, we reported a new strategy to overcome the above mentioned challenges. First, we chose CeO_x as the electrode material which is an interesting electronic material with unique physical and chemical properties, due to the existence of stable multiple oxidation states Ce (3+) and Ce (4+). We developed novel hierarchical nano-microstructures composed of self-assembled polycrystalline CeO_x nanocrystals without using any hard or soft templates but by the means of controlling nitrate ions oxidation rates. The fundamental charge-storage performances of CeO_x nano-microstructures were systematically investigated and nano-micro biscuits were found to exhibit superior performance over other structures. The second particularly imperative part of this work is to separate the capacitive behaviour from the diffusion-controlled intercalation behaviour by fitting the voltametric currents at various sweep rates to appropriate power law relationship. To the best of our knowledge, the present work is the first approach towards tuning the CeO_x morphologies via controlling nitrate ions oxidation rate. Moreover, there are hardly any reports which quantify the capacitive behaviour and intercalation effects in CeO_x based electrochemical capacitors. This study describes a new route for the synthesis of CeO_x nano-microstructures for self-powered energy storage and harvesting devices.

Materials and Methods

(a) Electrodeposition of CeO_x nano-micro structures

The growth of CeO_x nano-micro structures on fluorine-doped tin oxide (FTO) was carried out using an electrochemical deposition process, using an aqueous solution containing 0.01M Ce(NO₃)₃·6H₂O, 0.05M NH₄Cl and 0.05M KCl with a current density of 0.5 mA/cm² for 2 hours at 70°C by using an Autolab 302N Potentiostat as described in our previous reports^{8,9}. During electrochemical deposition synthesis, different volume ratios of ethanol to de-ionized (DI) water (10:90), (20:80), (30:70) and (40:60) respectively to prepare four different solvent solutions. A standard three-electrode setup in an undivided cell was used. F-doped tin oxide glass (FTO, 9.3~9.7 Ω, Asahi Glass Corporation, Japan, 1.1 mm×26 mm×30 mm) was used as the working electrode, while platinum foil (0.2mm×10 mm×20 mm) was used as the counter electrode. The distance between the two electrodes was 30 mm. The reference electrode was an Ag/AgCl electrode in 3 M KCl solution, against which all the potentials reported herein were measured.

(b) Characterization

The phase composition of the samples was characterized by X-ray diffraction (Philips X'pert Multipurpose X-ray Diffraction System (MRD) with Cu Kα) studies. The morphologies of the samples were observed by scanning electron microscopy (Nova Nano SEM 230) and transmission electron microscopy (Philips CM 200), respectively. The X-ray photoelectron spectroscopy (XPS) was performed in ESCALAB250Xi spectrometer using a monochromatized Al K alpha X-ray source (*hν*) 1486.6 eV with 20 eV pass energy.

The electrochemical characterization was carried out in a conventional three-electrode cell with 3 M KOH. The CeO_x nano-micro structures served as the working electrodes, Platinum foil as counter electrode and Ag/AgCl as reference electrode. All electrochemical

measurements were conducted with Autolab 302N electrochemical workstation controlled with Nova software. Cyclic voltammograms were measured at scan rates of 2.0 mVs^{-1} to 200 mVs^{-1} in a potential window range from 0 to 1 V. Galvanostatic charge/discharge curves were collected at the current density of 0.5 A/g . The surface depth profilometer (Dektak II) was used to determine the thickness of the electrodes and the thickness of CeO_x nano-micro biscuits were measured to be about $6\text{-}7 \text{ }\mu\text{m}$. The weights of all electrodes (mass loading) were determined by subtracting the weight of substrate from the films deposited on substrates by using microbalance. The Brunauer–Emmett–Teller (BET) surface area and pore size distribution of all samples were obtained from nitrogen physisorption isotherms (adsorption–desorption branches) at 77 K on a Micromeritics Tristar 3000 instrument. Prior to the measurements, the CeO_x samples were degassed overnight under vacuum at $150 \text{ }^\circ\text{C}$ to vaporize water molecules adsorbed on the CeO_x materials.

Results and Discussion

(a) Material Characterization

A series of electrochemical deposition experiments were performed with various concentrations of ethanol ($\text{CH}_3\text{CH}_2\text{OH}$) in solvents, while all other parameters remained unchanged. The as-prepared samples are re-named as; E-10, E-20, E-30 and E-40 corresponding to different volume ratios of ethanol to DI water (10:90), (20:80), (30:70) and (40:60) respectively. The surface morphologies of all synthesized CeO_x samples can be depicted from figures 1 and 2. The arrays of CeO_x nanowires vertical to substrate are depicted from figure 1a, which were synthesized by introducing 10% ethanol in the precursors. The high magnification image of nanowires arrays (as shown in the inset), reveals that these nanowires actually exist in the form of bunches.

By adding more ethanol (20%) in the solvent solution, CeO_x nanocables with slightly large diameter than nanowires ($\sim 250\text{nm}$) were formed as shown in figure 1b. The top of the nanocables is found to be coarse and consist of CeO_x nanoparticles (inset of figure 1b). The TEM image of a single CeO_x nanowire and the HRTEM of the particular spot are depicted from figure 1c and 1d. The lattice spacing is $\sim 0.31\text{ nm}$, corresponding to the (111) plane of the face-centred cubic (FCC) CeO_x .

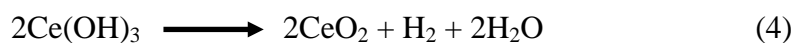
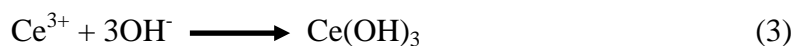
Hierarchical nano-micro biscuits (figure 2a) was obtained by adding 30% ethanol into the precursor solution. The high magnification image (figure 2b) reveals that these nano-micro biscuits are actually constructed by numerous brick-like nanoparticles, assembled in a *brick-upon-tile* pattern. Such a microstructure could be capable of offering some unique advantages such as; the well oriented brick-like nanocrystals within the individual biscuits provide active sites to maximize the capacitance locally. The brick-upon-tile structure can also provide excellent passage to the fast ions in the electrodes to facilitate the charge/discharge process. The TEM image of a single CeO_x biscuit can be depicted from figure 2c and the HRTEM of highlighted square region is shown in figure 2d, which reflects the polycrystalline nature of the nano-micro CeO_x biscuit. The selected area diffraction pattern as illustrated in figure 2e demonstrates the distinct circular rings pattern, hence confirms the formation of polycrystalline CeO_x with well identified characteristic planes. By further increasing the ethanol concentration in solvent to 40%, the nano-micro biscuits geometry was again transformed to cross-linked micro walls arrays as shown in figure 2f.

The SEM observations of the products reveal that the amount of added ethanol in the solvents is the key factor to control the morphology evolution of the CeO_x nano-microstructures. It is interesting to note that the morphology, the self-assembly pattern and the size of CeO_x particles highly depend on the amount of added ethanol in solvent solution and that can be manipulated by the superstructure assembled by nanowires, nano cables, nano-micro biscuits

to micro walls. The addition of ethanol may change the polarity, viscosity and solvency of the solvents, thus can induce different crystal growth habits. The polarity of solvents influences not only on the nucleation of the CeO_x crystals but also the preferential direction of the crystal growth^{10, 11}.

(b) Growth Mechanism

In general, the electrochemical synthesis of CeO_x is a four step-process: First, nitrate ions and H_2O are electrochemically reduced at the surface of the working electrode, resulting in an increase in local pH within the vicinity of the electrode (substrate) by following equation 1 & 2:



The increase in the local pH leads to the precipitation of cerium ions as cerium hydroxide by following equation (3) at room temperature. After exposure to air, even at room temperature, $\text{Ce}(\text{OH})_3$ can be transformed into CeO_x nuclei and H_2 . Once the concentration of CeO_x has reached super saturation, the CeO_x nucleates and grows into a layer of CeO_x particles as a seed layer for further growth of nanowires arrays (NWAs). By increasing deposition time, the nanorods gradually occur on the surface of the CeO_x seed layer and finally form the long nanowires arrays. These nanowires have low crystallinity and a quasi-polycrystalline nature. However, it is still evident from HRTEM image (figure 1d) and XRD pattern of E-10 (figure S1), that these nanowires grew along [220] direction as shown in upper panel of figure 3.

For low ethanol concentration in the precursors, the nucleation rate is faster as nitrate ions get oxidized much faster to produce OH^- as compared to the case of excessive ethanol. Therefore, most of the substrate surface can be fully covered by the CeO_x nuclei, thus facilitating the oriented growth of dense nanowire arrays to the substrate. By increasing the ethanol concentration, CeO_x nuclei only form on a part of the substrate surface, creating the space for lateral growth after the formation of nanowires with a certain length. The CeO_x nanowires composed of polycrystalline nanoparticles and the nucleation is purely controlled by a constant current density, so the continuing nucleation/growth of CeO_x nanoparticles on the top of the CeO_x nanowires becomes more difficult. The further increase in the length of the nanowire may cause overall resistance of the nanowires to impede the nucleation on the upper side of nanowires. This facilitates the lateral growth due to relatively lower resistance on the side surface of nanowires. Also, due to the limited availability of nucleation sites on the substrate (slow nitrate oxidation process due to excessive ethanol), the propagation of peer group lateral sites cannot be ruled out which transform the CeO_x morphologies from nanowires to nanocables, nano-micro biscuits and finally to micro walls (schematically demonstrated in the lower panel of figure 3).

To verify the above mentioned phenomenon, X-ray diffraction studies with the aid of potential-time variations and ex-situ SEM studies were described in figures S1, S2 and S3 respectively. From figure S1, it can be seen that the E-10 has the strongest (220) peak, suggesting a preferable oriented growth along the normal direction to the substrate (nanowires). Such a growing behaviour is suppressed by increasing ethanol concentration from E-20 to E-40. However, the strong (111) diffraction peak of E-30 and E-40 indicates the preferable nucleation growth in lateral direction, thus leading to the formation of nano-micro biscuits and micro walls.

(c) Electrochemical Characterization

For the evaluation of the redox behaviour, the CV measurements were conducted at two different scan rates of 5mV/s and 100mV/s. To appliance these measurements, all CeO_x nanocrystals were used as the working electrodes, platinum foil as the counter electrode and Ag/AgCl as the reference electrode with the presence of 3 M KOH as the electrolyte in the potential window of 0.0 to 1.0 V (figure 4a and 4b).

The potential window is chosen to avoid the occurrence of oxygen evolution reaction. The larger loop area of the CV curve indicates the higher specific capacitance. Among the four samples, E-30 shows the highest peak current density and the largest loop area under both scan rates (5 mV/s and 100 mV/s), indicating the largest electrochemical capacitance. Furthermore, its peak current density remains more stable than that of the other three samples in a large potential range. These characteristics demonstrate the superior capacitive performance of the E-30 electrode. The charge/discharge curves of all CeO_x nanocrystals at the current density of 0.5A/g are also illustrated in figure 4c. The E-30 electrode exhibited the longest discharge time and the highest specific capacitance, which is in good agreement with the CV measurement.

The charge storage kinetics among all CeO_x based nano-microstructures are quantified by their charge storage capabilities at a given time over a potential window of 0.4V as shown in figure 4d. As depicted from C-V measurements (figures 4a and 4b), nearly all CeO_x nano-microstructures attained their peak current densities at ~0.4V, therefore for evaluating their charging capabilities, the potential window of 0.4V was chosen. As expected, the highest capacity is achieved for the E-30 samples: at a charging time of only 100s the capacity is approximately 275 Cg⁻¹, corresponding to a specific capacitance of 650 Fg⁻¹. As charging time increases, the capacity increases until it achieves a consistent value of 300 Cg⁻¹ after ~ 2.5 minutes. The other samples (E-10, E-20 and E-40) also show significant charge storage

capabilities, but their values are much lower than E-30, despite the fact that the surface area and total pore volume of the E-30 is significantly larger than rest of electrodes (as can be seen from figure 2 and supporting information table 1). Furthermore, the rapid charge storage kinetics in E-30 suggests towards the possibility of faradaic contribution in charge storage process, where the diffusion-related processes are expected to be minimal.

The long-term cycling stability during charging-discharging process is very important for energy source material, especially for supercapacitor electrode materials. The cycling stability of all fabricated CeO_x nano-microstructures was tested and among them, E-30 exhibits excellent capacitance retention (100% retention for the first 1800 cycles) and retains its 89% of retention after 3000 cycles (Figure S4). Moreover, the nan-micro biscuits retained its structural stability after 3000 cyclic tests as depicted from figure S5. Such retention capability is superior to previously reported CeO_x -based asymmetric supercapacitors, such as CeO_2 hexagonal nanoplates (19 % loss for first 2000 cycles)¹², carbon coated CeO_2 (9.6 % loss after 2000 cycles)¹², and NiO-CeO_2 (9 % loss during first 200 cycles)¹³. The life time of CeO_2 nanoparticles/graphene nanocomposite was only reported as 1000 cycles¹⁴. This impressive cyclic retention performance of E-30 may be attributed to the interconnected nano-micro biscuits with mesoporous nanostructures which may shorten the ion and electron diffusion paths, hence serve as an ideal platform for supercapacitive energy storage.

(d) Charge storage contribution

In order to investigate the actual amount of charge storage capacity of E-30, a quantitative analysis on total charge storage capacity for E-30 was adopted which was previously utilized by some other reports as well^{15, 16}. According to this analysis, there are two main sources which mainly contribute to the overall charge storage capacity (Q) of any material. The first contribution comes from the outer surface called “Capacitive charge storage, the most

accessible surface (Q_{outer})” and the other originate from the inner surface called “bulk charge storage, the less accessible (Q_{inner})”.

$$Q = Q_{outer} + Q_{inner} \quad (1)$$

As, the bulk charge storage (Q_{inner}) depends upon ion diffusion process, therefore, the relationship between voltage sweep rate and charge capacity could be a key tool to establish the rate limited step of a charge-storage mechanism. So, by assuming the ion diffusion process as semi-infinite linear diffusion, one can expect the variation in Q_{inner} with $t^{1/2}$. By rewriting the above equation in terms of the voltage sweep rate (v), the following relationship arises:

$$Q(v) = Q_{outer} + constant(v^{-1/2}) \quad (2)$$

The charge storage capacity with corresponding capacitances for E-30 was recorded and plotted with various voltage sweep rates in figure 5a. It can be clearly seen that the normalized charge tend to decrease with increasing sweep rate so does the capacitance too. In the plot of charge capacity vs. $v^{-1/2}$, a straight line is expected, whose y-intercept ($v = \infty$) estimates the contribution of storage capacity comes from the outer surface or the infinite-sweep rate capacity.

The plot of normalized capacity/gravimetric capacity versus $v^{-1/2}$ for E-30 from 2 to 200 mV s^{-1} which can be divided in two regions depending on sweep rates is depicted in figure 5b. The region-1 corresponds to low and intermediate sweep rates, where linear relationship between sweep rate and capacity storage is emerged. However, at high sweep rates (region-2), the capacity mostly remains independent of sweep rates. Usually, this deviation from straight line could be attributed to the possible emergence of polarization effects at high sweep rates. Therefore, low and intermediate sweep rates are then selected to extrapolate to the y-intercept. This value represents the amount of charge storage from capacitive processes (contribution from outer surface), namely double-layer and/or pseudo capacitance. At slow

sweep rates, diffusion-related processes begin to contribute and the total amount of charge storage becomes a combination of capacitive and diffusion components¹⁷. In some materials, diffusion-related charge storage (contribution from inner surface) increases significantly and far outweighs the capacitive contribution. In the case of E-30 at lower sweep rates ($\sim 2 \text{ mV s}^{-1}$), the diffusion process contribute about 35% of the total charge capacity which decreases with increasing sweep rate and its contribution remains only about 4% at 100 mV s^{-1} as shown in figure 6. Our results on the basis of capacitance distribution are far superior than previously reported TiO_2 nanoparticles based electrochemical capacitors in which diffusion processes contributed between 85% and 45% of the total amount of charge storage¹⁸.

(e) Charge Storage Phenomenon

The excellent electrochemical performance of the CeO_x nano-micro biscuits (E-30) are mainly attributed to the loosely packed structure of nano-micro biscuits, which allow better accessibility of the electrolyte ions. Also, the nano-micro biscuits are mainly comprised of CeO_x nanoparticles assembled in a *brick-upon-tile* pattern, therefore offering a larger surface areal zone for ion diffusion and electron transport during the charge/discharge process. Hence good electrochemical utilization of CeO_x nano-micro biscuits is evidenced.

In addition, the concentration of Ce^{3+} ions is also responsible to drive the redox reaction in ceria based electrochemical cells. To estimate the concentration of Ce (3+) and Ce (4+) contents in both E-10 and E-30 samples, XPS studies were conducted and the corresponding Ce 3d spectra are presented in figure S6. The XPS spectra of Ce 3d can be assigned to the different spin orbit states of $3d_{3/2}$ (Peaks with label-U) and $3d_{5/2}$ (peaks with label-V). The peaks denoted by V_1 , V_3 , U_1 and U_3 are characteristic peaks of Ce^{3+} ions, whereas those marked by V_2 , V_4 , U_2 and U_4 are of Ce^{4+} ions. The deconvoluted Ce(3d) spectra is relatively complex due to the presence of Ce in 3+ and 4+ oxidation states as well as multiple d-splitting ($3d_{3/2}$ and $3d_{5/2}$)¹⁹.

Therefore, the appearance of peaks in the XPS spectra of the Ce 3d level associated with the mixture of Ce^{3+} and Ce^{4+} oxidation states indicates their coexistence in both E-10 and E-30. Recent studies showed the Ce^{3+} indirectly represents oxygen vacancies in the lattice and these oxygen vacancies on ceria nanoparticles play an important role in improving the electrical and electrochemical properties²⁰. The presence of higher Ce^{3+} content in E-30 indirectly refers to availability of more non-stoichiometric oxygen to boost redox reaction, thus results in better electrochemical performance. Also, the ratio $\text{Ce}^{3+}/\text{Ce}^{4+}$ in E-30 (0.294) was found almost twice higher than that of E-10 (0.177), indicating higher concentration of non-stoichiometric oxygen in E-30 are available to drive faradaic redox reactions.

Generally, CeO_x is not considered to be an ideal candidates for electrochemical capacitors by having electronically insulating (dielectric constant ~ 26 and high electrical resistivity) nature with wide bandgap of ~ 3.6 eV. However, the excellent electrochemical performances of our CeO_x nano-micro biscuits can be attributed to its unique *brick-upon-tile* patterned geometry. The insertion of potassium ions (from electrolyte solution) into the structure apparently dopes the material and increases its electronic conductivity. Electrochemical impedance measurements of E-30 sample before and after its exposure to potassium ions (Potassiation) were carried out and shown in figure S7. It can be clearly perceptible that the charge transfer resistance decreases by three orders of magnitude after potassiation, thus reduces the ionic diffusion resistance and thereby, enhances the redox kinetics. There may be several other factors that could influence the electronic conductivity of these materials during potassiation and their investigations would provide a future direction of study.

A number of approaches have been devolved to optimize the specific capacitance of various electrodes. One of the effective approaches is to develop three-dimensional (3D) hierarchical porous nanostructure. This not only provides a continuous electron pathway, but also facilitates ion transport by shortening diffusion pathways^{21, 22}. For example, Wang et al.¹⁴

exploit CeO_x nanoparticles/graphene nanocomposite, Rakhi et al.²¹ utilize MnO_2 nanoflowers onto carbon nanotubes, Vijayakumar et al.²³ fabricate NiO/Carbon nanocomposite and Ghimbeu et al.²⁴ proposed Vanadium nitride/CNT to enhance the supercapacitive performances of the cells. We also fabricated CeO_x nano-micro biscuits (E-30) on carbon foam by following the previously described method to evaluate the performance of CeO_x nano-micro biscuits (E-30)/Carbon foam composite. The surface morphology of carbon foam in both low and high magnification is shown in Figure S8 of the supporting information. The corresponding Galvanostatic charge-discharge curves of E-30/Carbon foam composite at 0.5A/g and pristine carbon foam are plotted in Figure 7.

The E-30/Carbon foam composite demonstrated far superior charge/discharge performances and retains its capacitance for 4000 cycles over E-30@FTO electrode. Various factors such as the electrode materials, the appropriate operating voltage, as well as the right selection of electrolyte could be responsible to attain such an impressive cycling stability of the asymmetric supercapacitors. Besides, the component of carbon foam in E-30@Carbon foam can effectively prevent the partial dissolution of CeO_x in the electrolyte solution and also enhance the mechanical strength, which can alleviate degradation of specific capacitance value upon cycling²⁵. The E-30 coated on carbon foam may also be able to accommodate the structural/mesostructural changes induced by the guest ions during the intercalation and de-intercalation process to improve the cycling stability. Moreover, porous 3D electrode allows more electroactive sites exposed to the electrolyte and providing hierarchical pathways for effective ion transport.

Conclusions

In summary, we have demonstrated a general paradigm for fabricating novel ceria based morphological features by implementing a simple and versatile electrochemical approach for

electrochemical energy storage capacitors. The ethanol addition in solvents during deposition process was ascertained to have strong impact for constructing various CeO_x nano-microstructures. The significant difference between the E-30 and other fabricated electrodes in terms of electrochemical behaviour arises from the fast faradaic reactions in E-30 that may leads to its additional pseudocapacitive storage capacity. A quantitative analysis shows less contribution comes from the diffusion effect in the overall charge storage capabilities of these nano-microstructures. The magnitude of electronic conductivity upon K^+ ions insertion and the means by which electronic conduction develops in this wide bandgap semiconductor remain to be addressed. Also, this work points towards future direction for the exploration of advanced electrochemical electrode materials that become highly conductive during ion intercalation.

Acknowledgments

The authors would like to acknowledge the financial support from the Australian Research Council Projects of DP140104373, DP150103006 and FT140100032.

References

1. Simon, P.; Gogotsi, Y. *Nat Mater* **2008**, 7, (11), 845-854.
2. Chen, Z.; Augustyn, V.; Wen, J.; Zhang, Y.; Shen, M.; Dunn, B.; Lu, Y. *Advanced Materials* **2011**, 23, (6), 791-795.
3. Zhang, L. L.; Zhao, X. S. *Chemical Society Reviews* **2009**, 38, (9), 2520-2531.
4. Miller, J. R.; Simon, P. *Science* **2008**, 321, (5889), 651-652.
5. Conway, B. E.; Birss, V.; Wojtowicz, J. *Journal of Power Sources* **1997**, 66, (1-2), 1-14.

6. Qu, Q.; Yang, S.; Feng, X. *Advanced Materials* **2011**, 23, (46), 5574-5580.
7. Liu, R.; Duay, J.; Lee, S. B. *Chemical Communications* **2011**, 47, (5), 1384-1404.
8. Younis, A.; Chu, D.; Li, S. *Journal of Materials Chemistry C* **2014**, 2, (48), 10291-10297.
9. Younis, A.; Chu, D.; Li, S. *Applied Physics Letters* **2013**, 103, (25), 253504.
10. Yin, J.; Gao, F.; Wei, C.; Lu, Q. *Sci. Rep.* **2014**, 4.
11. Kunjara Na Ayudhya, S.; Tonto, P.; Mekasuwandumrong, O.; Pavarajarn, V.; Praserthdam, P. *Crystal Growth & Design* **2006**, 6, (11), 2446-2450.
12. Padmanathan, N.; Selladurai, S. *RSC Advances* **2014**, 4, (13), 6527-6534.
13. Padmanathan, N.; Selladurai, S. *Ionics* **2014**, 20, (3), 409-420.
14. Wang, Y.; Guo, C. X.; Liu, J.; Chen, T.; Yang, H.; Li, C. M. *Dalton Transactions* **2011**, 40, (24), 6388-6391.
15. Ardizzone, S.; Fregonara, G.; Trasatti, S. *Electrochimica Acta* **1990**, 35, (1), 263-267.
16. Kim, J. W.; Augustyn, V.; Dunn, B. *Advanced Energy Materials* **2012**, 2, (1), 141-148.
17. Baronetto, D.; Krstajić, N.; Trasatti, S. *Electrochimica Acta* **1994**, 39, (16), 2359-2362.
18. Wang, J.; Polleux, J.; Lim, J.; Dunn, B. *The Journal of Physical Chemistry C* **2007**, 111, (40), 14925-14931.
19. Kumar, A.; Babu, S.; Karakoti, A. S.; Schulte, A.; Seal, S. *Langmuir* **2009**, 25, (18), 10998-11007.
20. Joung, D.; Singh, V.; Park, S.; Schulte, A.; Seal, S.; Khondaker, S. I. *The Journal of Physical Chemistry C* **2011**, 115, (50), 24494-24500.
21. Rakhi, R. B.; Chen, W.; Cha, D.; Alshareef, H. N. *Advanced Energy Materials* **2012**, 2, (3), 381-389.

22. Chen, Z.; Ren, W.; Gao, L.; Liu, B.; Pei, S.; Cheng, H.-M. *Nat Mater* **2011**, 10, (6), 424-428.
23. Vijayakumar, S.; Nagamuthu, S.; Muralidharan, G. *ACS Sustainable Chemistry & Engineering* **2013**, 1, (9), 1110-1118.
24. Ghimbeu, C. M.; Raymundo-Pinero, E.; Fioux, P.; Beguin, F.; Vix-Guterl, C. *Journal of Materials Chemistry* **2011**, 21, (35), 13268-13275.
25. Yan, J.; Wang, Q.; Wei, T.; Fan, Z. *Advanced Energy Materials* **2014**, 4, (4), 1300816.

Figures Captions:

Figure 1: (a) FESEM micrograph of CeO_x nanowires (E-10) (inset is the high magnification image) (b) SEM image of CeO_x nanocables (E-20) (inset is the high magnification image) (c) TEM image of a single CeO_x nanowire (d) HRTEM of selected white square showing lattice spacing.

Figure 2:(a) SEM of CeO_x nano-micro biscuits (E-30) at low magnification (b) SEM of CeO_x nano-micro biscuits at high magnification (c) TEM image of a CeO_x nano-micro block (d) HRETM of selected highlighted square of nano-micro block (e) SAED pattern of highlighted region showing polycrystalline nature (f) Low magnification image of CeO_x micro walls (E-40).

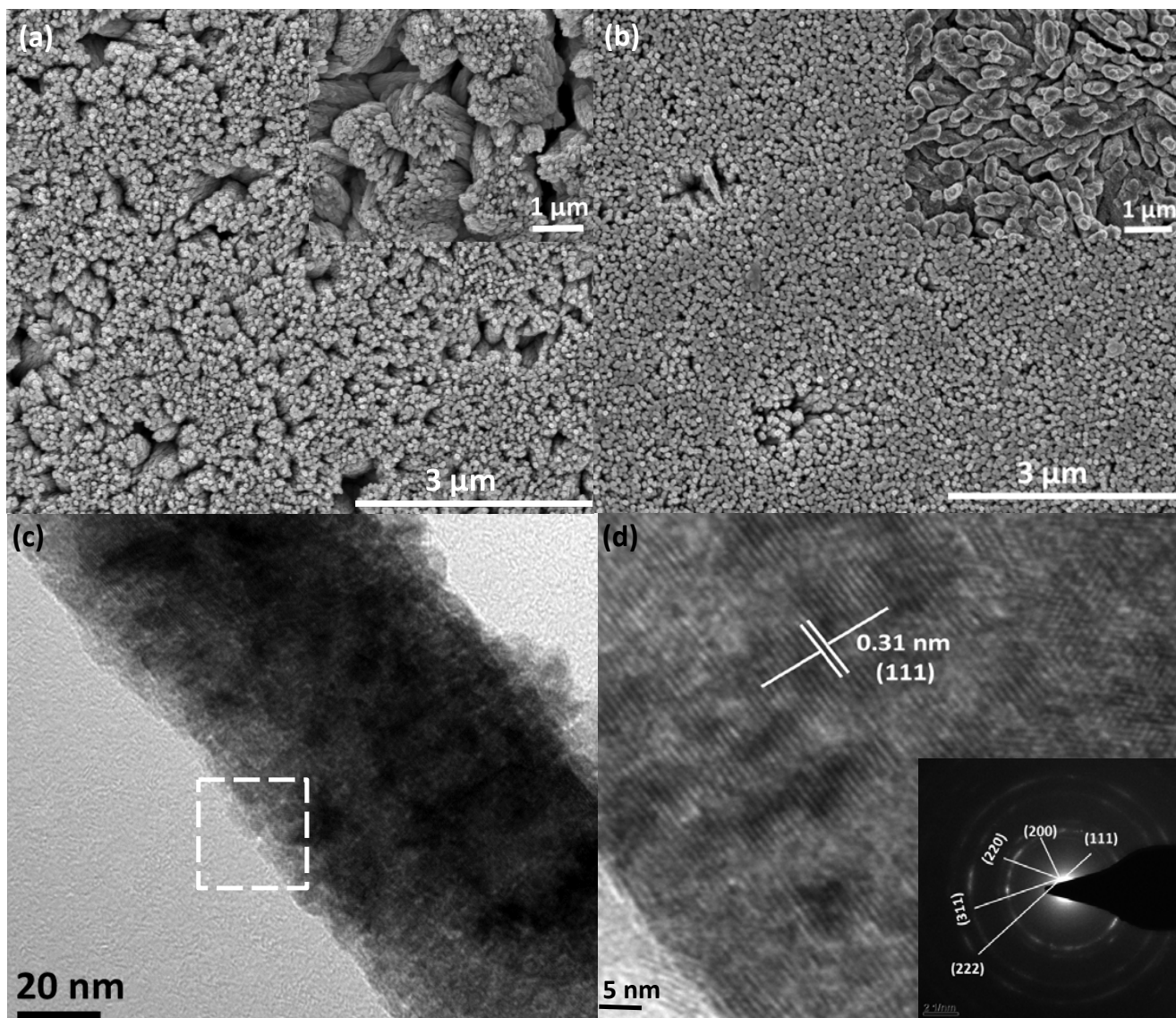
Figure 3: Growth mechanism of various CeO_x nano-microstructures with different concentration of ethanol in precursors.

Figure 4: Electrochemical tests: (a) CV curves of all samples at scan rate of 5mVs⁻¹, (b) CV of different samples at 100mVs⁻¹ scan rate, (c) Galvanostatic charge–discharge curves of all samples (E-10, E-20, E-30 and E-40) at current density of 0.5 A/g, (d) Charge storage as a function of charging time for all samples (E-10, E-20, E-30 and E-40) at fixed potential of 0.4V. The E-30 demonstrates the highest level of charge storage capacity among all samples

Figure 5: (a) The variation in capacity/gravimetric capacitance of E-30 with voltage sweep rates. (b) The capacity as a function of sweep rate^{-1/2}, the y-intercept is 170.58 C g⁻¹ and represents the infinite sweep rate capacity (contribution from capacitive charge storage /outer surface).

Figure 6: The contribution of the capacity at infinite sweep rate to the total charge-storage for all sweep rates.

Figure 7: (a) Galvanostatic charge-discharge curves of carbon foam and E-30@carbon foam at 0.5A/g (b) Variation of specific capacitance retention as a function of cycle numbers..

**Figure 1**

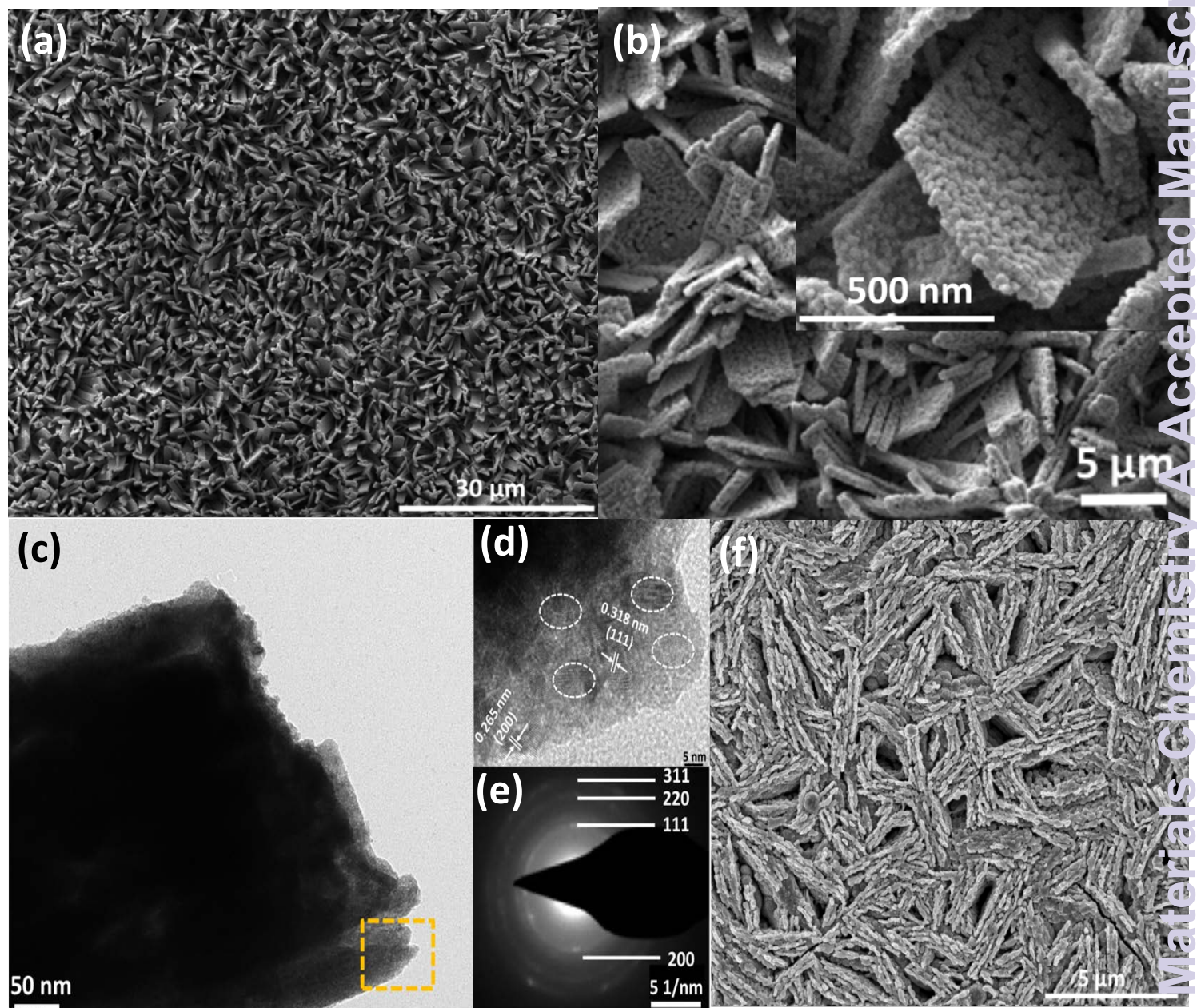
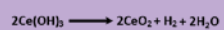
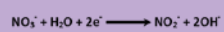


Figure 2

Low ethanol concentration


Nucleation



Formation of CeO₂ nanowires

Oriented Growth

CeO₂ nanowires array

 Nucleation site

High ethanol concentration

Nucleation

Formation of CeO₂ nano-micro biscuits

Lateral Growth

CeO₂ nano-micro biscuits

Figure 3

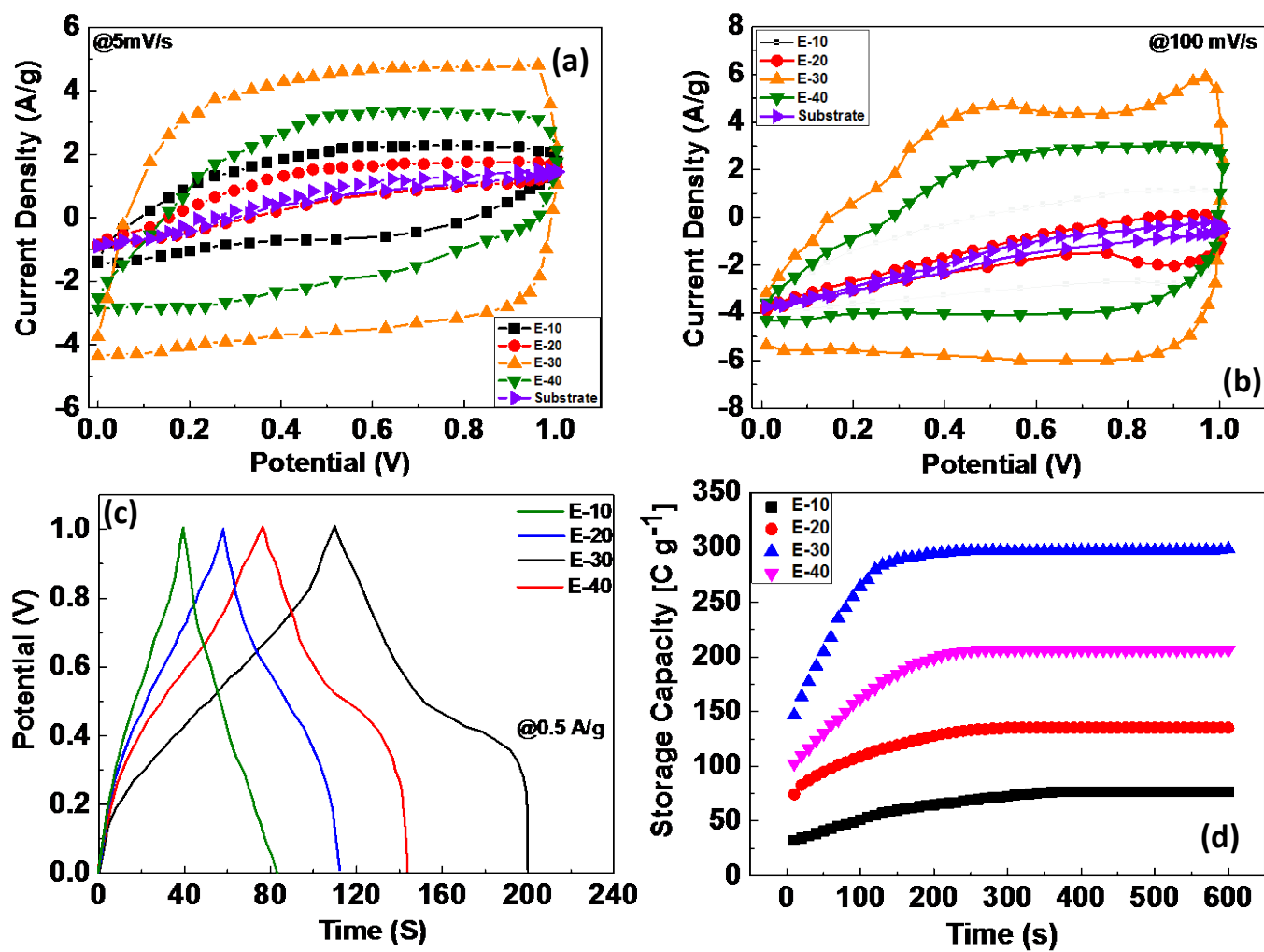


Figure 4

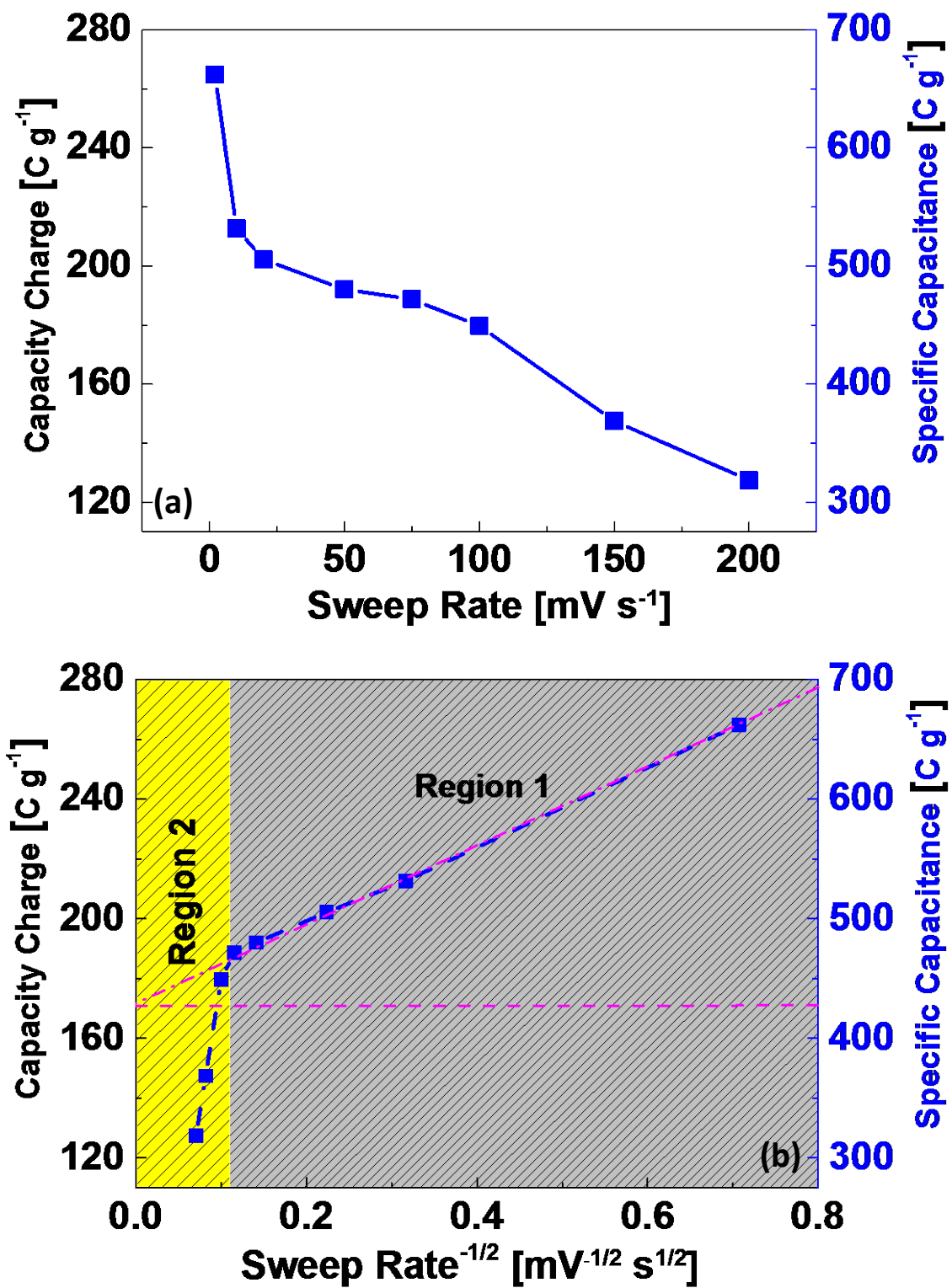


Figure 5

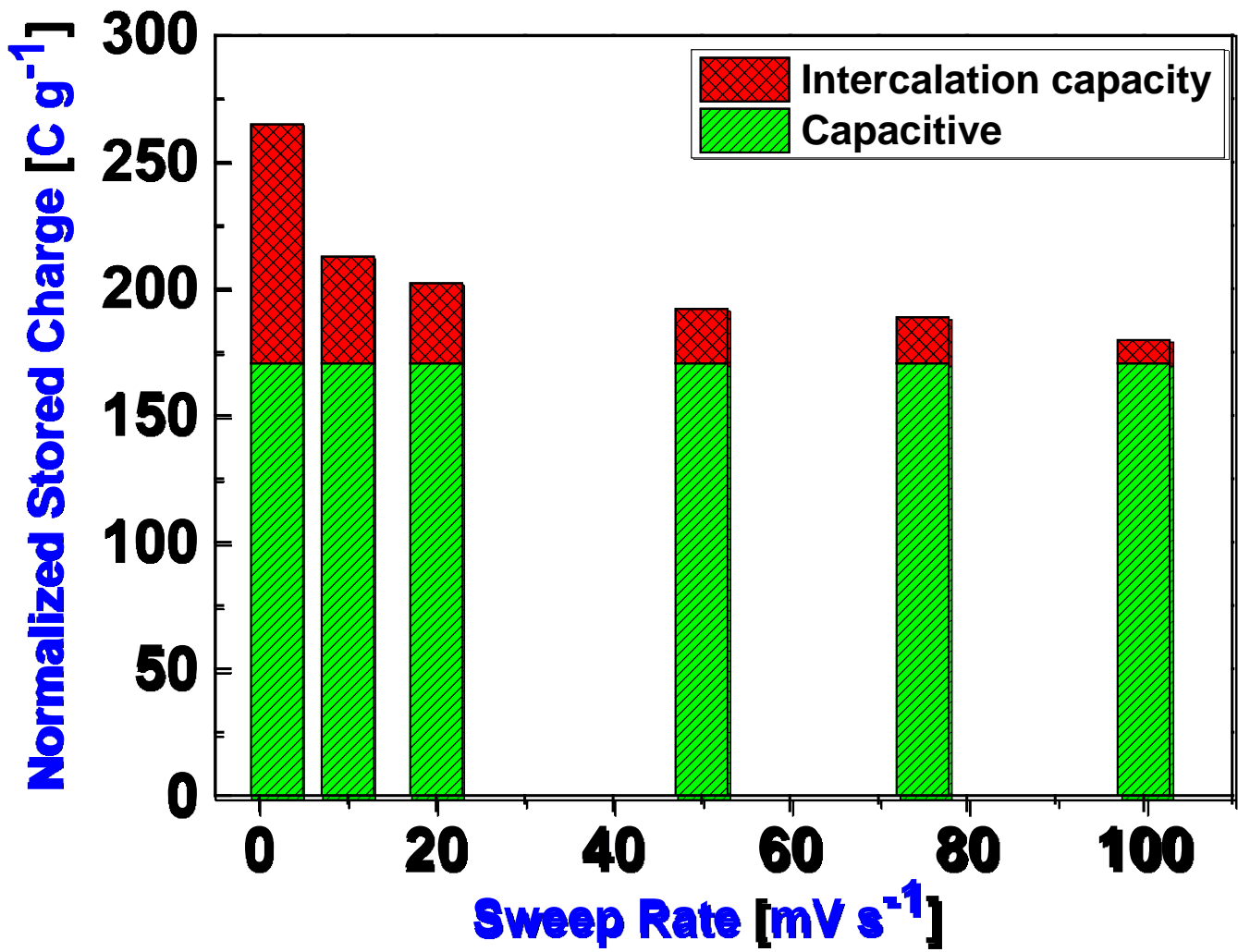


Figure 6

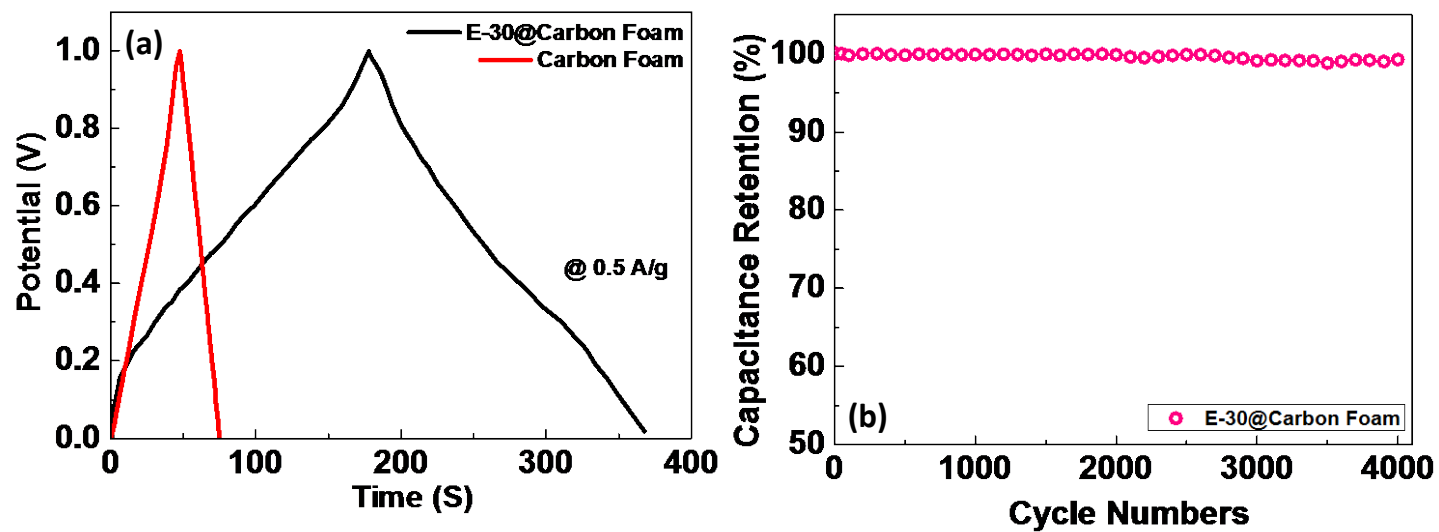


Figure 7

Table of Content

A facile and versatile electrochemical synthesis route was adopted to construct various CeO_x hierarchical nano-microstructures for advanced electrochemical capacitors.

